

## Multi-objective optimization of surface roughness, cutting forces, productivity and Power consumption when turning of Inconel 718

Hamid Tebassi<sup>a\*</sup>, Mohamed Athmane Yallese<sup>a</sup>, Riad Khettabi<sup>a</sup>, Salim Belhadi<sup>a</sup>, Ikhlas Meddour<sup>a</sup> and Francois Girardin<sup>b</sup>

<sup>a</sup>Laboratory of Mechanics and Structures (LMS), May 8th 1945 University, P.O. Box 401, Guelma 24000, Algeria

<sup>b</sup>Laboratoire Vibrations Acoustique, INSA-Lyon, 25 bis avenue Jean Capelle, F-69621 Villeurbanne Cedex, France

### CHRONICLE

#### Article history:

Received April 22 2015

Received in Revised Format

July 23 2015

Accepted July 23 2015

Available online

July 23 2015

#### Keywords:

Surface roughness

Productivity

RSM

Box-Cox tool

Response optimization

Desirability

### ABSTRACT

Nickel based super alloys are excellent for several applications and mainly in structural components submitted to high temperatures owing to their high strength to weight ratio, good corrosion resistance and metallurgical stability such as in cases of jet engine and gas turbine components. The current work presents the experimental investigations of the cutting parameters effects (cutting speed, depth of cut and feed rate) on the surface roughness, cutting force components, productivity and power consumption during dry conditions in straight turning using coated carbide tool. The mathematical models for output parameters have been developed using Box-Behnken design with 15 runs and Box-Cox transformation was used for improving normality. The results of the analysis have shown that the surface finish was statistically sensitive to the feed rate and cutting speed with the contribution of 43.58% and 23.85% respectively, while depth of cut had the greatest effect on the evolution of cutting force components with the contribution of 79.87% for feed force, 66.92% for radial force and 66.26% for tangential force. Multi-objective optimization procedure allowed minimizing roughness Ra, cutting forces and power consumption and maximizing material removal rate using desirability approach.

## Nomenclature

Vc	Cutting speed (m/min)
f	Feed rate (mm/rev)
ap	Depth of cut (mm)
r <sub>ε</sub>	Tool nose radius (mm)
Fa	Feed force (N)
Fr	Thrust force (N)
Fv	Tangential force (N)
Kc	Specific cutting force
Ra	Arithmetic mean of roughness (μm)

\* Corresponding author. Tel: +213 662031397

E-mail: [tebassihamid@yahoo.fr](mailto:tebassihamid@yahoo.fr) (H. Tebassi)

$a_{ii}$	<i>Quadratic terms</i>
$a_i$	<i>Coefficients of linear terms</i>
$a_{ij}$	<i>Cross-product terms</i>
DF	<i>Combined desirability function</i>
$R^2$	<i>Determination coefficient</i>
ANOVA	<i>Analysis of variance</i>
RSM	<i>Response surface methodology</i>
Df	<i>Degrees of freedom</i>
Cont.%	<i>Percentage contribution ratio (%)</i>
MRR	<i>Material removal rate (<math>cm^3/min</math>)</i>
Pc	<i>Power (watt)</i>
$\alpha$	<i>Clearance angle, degree</i>
$\chi_r$	<i>Major cutting edge angle, degree</i>
$\gamma$	<i>Rake angle, degree</i>
$\lambda$	<i>Cutting edge inclination angle, degree</i>
HRC	<i>Workpiece hardness</i>
$\Omega$	<i>Desired response</i>
$X_i$	<i>Coded variables</i>
$\lambda$	<i>Power law transformation</i>

## 1. Introduction

The Inconel is one of the most important materials used in the modern industries. In addition of the best properties in terms of high strength, corrosion resistance, heat resistance and fatigue resistance, the Inconel 718 has, also a low thermal conductivity (Lynch, 1989). Generally, this type of alloy is difficult to machine for the following reasons (Alauddin et al., 1996): High work hardening rates at machining, strain rates leading to high cutting forces; abrasiveness; toughness, gummy and strong tendency to weld to the tool with forming the built-up edge; low thermal properties leading to high cutting temperatures. However, it has a wide variety of applications such as aircraft gas turbines stack gas reheaters, reciprocating engines, etc. For those special material properties, high cutting force, tool wear, and cutting temperature are the main characteristic features in the machining process. Surface integrity is relatively an important term used to describe the nature or condition of the surface region of a component (Sadat, 1987). In the study of wear behavior of nano-multilayered coatings, Biksa et al. (2010) obtained that the metallurgical design of the nano-multilayered coating should be tailored to its application and to achieve better tool life when machining aerospace alloys and the adaptive nano-multilayered AlTiN/MoN coating was recommended. A review of developments towards dry and high speed machining of Inconel 718 alloy, by Dudzinski et al. (2004) shows that the higher cutting speeds under dry conditions, certainly up to 100 m/min, may be carried out with coated carbide tools. Settineri et al. (2008) investigated properties and performances of innovative coated tools in turning aerospace alloy Inconel 718 and obtained that the all tested tools performed better than the uncoated inserts.

An interesting work investigates the cutter orientation of the Ball Nose end milling of the Inconel 718, carried out by Ng et al. (2000), found that the TiAlN coating performed better than the CrN coating due to the former having higher oxidation resistance, higher hardness and a lower coefficient of friction. In the investigation of the cutting process effect on machining performance and surface integrity with coated and uncoated carbide tools (Outeiro et al. 2008), results show that higher surface residual stresses are generated when machining of Inconel 718 with the uncoated tool than the coated tool. Furthermore, when machining the age hardened Inconel 718 with the coated carbide tools, Arunachalam et al. (2004) found that finishing operations may not produce a high value of compressive residual stresses and may sometimes even generate tensile residual stresses if the radial cutting length is more than 30 mm.

When faced milling of Inconel 718 aerospace alloy, Jawaid et al. (2001) obtained that the PVD TiN coated tools award a better performance than the uncoated tool at cutting speed of 50 m/min and feed rate of 0.08 mm per tooth. Results of machinability investigation of Inconel 718 (Rahman et al., 1997), indicated that the allowable speed and feed ranges for machining Inconel 718 were at notably low levels and tool life of the inserts decreased when the speed or the feed was increased; this is due to the commonly experienced high cutting forces, low thermal conductivity, abrasiveness and work hardening tendencies of work material, resulting in high heat generated at the cutting edge.

However, Nalbant et al. (2007) obtained that the minimum average surface roughness was determined with single layer TiN coated cemented carbide tools while maximum average surface roughness was observed with multicoated Al<sub>2</sub>O<sub>3</sub> tools. The carbide insert used by Thakur et al. (2009) during turning of the Inconel 718 shows that the surface finish was optimum in the cutting speed range of 45 to 55 m/min for low feed rate and depth of cut; cutting force magnitude was found higher than feed force. However, the surface roughness could be also affected by the cutting conditions. The increase of the cutting speed  $V_c$  should improve the surface roughness by the surface softening. At the high cutting speed, the deformation rate in the workpiece surface was increased by increased temperature causing the surface softening and by consequence, improved surface roughness and the surface roughness were also affected by the feed rate (Ståhl et al., 2011). During a study of machinability assessment of Inconel 718 accomplished by Choudhury and El-Baradie (1999), it was revealed that the surface roughness generated by the uncoated and coated tools was mostly influenced by the change in feed, and the increase in the depth of cut improved the surface finish produced by the coated carbide tools whilst it was the opposite when the uncoated tools were used while cutting force was decreased when the speed was increased and increased when the feed or depth of cut was increased.

In order to model responses and input parameters optimization in dry turning of Inconel 718 using coated carbide inserts, Ramanujam et al. (2014) found that the feed rate was the most significant parameter impacting surface roughness, followed by depth of cut and cutting speed. The examination of the effect of high-pressure coolant supply when machining Inconel 718 concluded that surface roughness obtained with coated carbide tool vary marginally with prolong machining, due probably to the gradual wear generated at the tool edge as well as temperature reduction at the cutting interface by the high coolant pressure employed (Ezugwu & Bonney, 2004).. Built-up edge deposition on the machined surface in dry conditions of Inconel 718 was due to the higher temperatures generated (Devillez et al., 2011). Machining parameters optimization in end milling of Inconel 718 super alloy using taguchi based grey relational analysis Maiyar et al. (2013) showed that optimal cutting parameters for the machining process lies at 75 m/min for cutting velocity, 0.06 mm/tooth for feed rate and 0.4 mm for depth of cut, this led to an increase of 64.8% in material removal rate and at the same time a decrease of 9.52% in surface roughness.

During machining the Inconel 718, a white layer can be generated, Bushlya et al. (2011) characterized this white layer when turning the aged Inconel 718 under a wide range of process conditions. They obtained that white layer was found to consist of nanocrystalline grains with grain size of 50-150 nm. Furthermore, at dry high-speed turning of Inconel 718, Pawade et al. (2007) found that the magnitude of cutting forces was two to three times higher than that of the other force components.

When end milling of Inconel 718 using coated carbide tool, force variation ranges overlapped between successive cuttings passes (Li et al., 2006). Along with the tool wear propagation in successive cutting passes, the overall trend of the main peak values in the X-, Y-, and Z- directions for both the down and up milling operations was in a gradual increase. Wear mechanisms investigation during drilling of Inconel 718 super alloy showed that the friction force was found to be the most important factor governing tool failure (Chen & Liao, 2003). Using new tools, Sharman et al. (2015) obtained that an increase in tool nose radius from 2 to 6 mm resulted in greater levels of plastic deformation.

Krain et al. (2007) optimized tool life and productivity when end milling Inconel 718, found that the best balance of tool life and productivity using M30 grade WC inserts was achieved when cutting at an immersion ratio of 50% and a chip thickness of 0.1 mm and the average metal removed was 21,406 mm<sup>3</sup> in 7.60 min, which resulted in a MRR of 2784 mm<sup>3</sup>/min.

Regarding the cited machining problematic, the main objective of the present work is to investigate the influence of different machining parameters on surface finish, cutting forces, productivity and power consumption when turning of Inconel 718 super alloy, because those later are highly essentials for functional requirements of products and economic state of industries. Response surface methodology design approach was utilized for experimental planning during turning of Inconel alloy. The results were analyzed to determine the optimal machining parameters settings and achieved optimal surface roughness, cutting forces, power consumption, and material removal rate. ANOVA was performed to investigate the more influencing parameters on the multiple performance characteristics. The mathematical model has been developed and normality was proved using Box-Cox transformation (Sakia, 1992; Osborne, 2010). Multi-objective optimization procedure allowed minimizing roughness Ra, cutting forces and power consumption with maximizing of material removal rate using desirability approach. Confirmation tests were performed by using experiments.

## 2. Material and methods

### 2.1 Materials and measurement

The aim of the current experimental work is to investigate the effect of cutting parameters on surface roughness, cutting force components, material removal rate and power consumption with, developing a correlation between them. In order to reach this objective, cutting speed, feed rate and depth of cut are chosen as process parameters. The workpiece material used in this study was Inconel 718 having hardness of 30 HRC and the chemical composition is: 0.08%C; 0.35%Mn; 0.35%Sn; 0.015%P; 0.015%S; 55%Ni; 21%Cr; 1%Co; 20%Fe; 3.3%Mo; 1.15%Ti; 0.15%Cu; 0.8%Al; 5.5% (Cb+Ta). The workpiece geometry is a cylindrical bar specimen with the diameter of 65 mm and the length of 350 mm. Straight turning operations have been achieved using a 6.6 kW spindle power TOS TRENCIN model SN40C lathe, during dry conditions. The experimental setup is shown in Fig.1.

Cutting inserts were coated carbide (Settineri et al., 2008; Jawaid et al., 2001), with the standard designation (ISO) of SNGN 1204 with radius nose of 0.8 mm, commercialized by Sandvik under GC1025 (Sandvik, 2009). The tool holder used in this experimental study has the standard designation of CSBNR2525M12 with the following angles:  $\chi_r = 45^\circ$ ,  $\alpha = 6^\circ$ ,  $\gamma = -6^\circ$  and  $\lambda = -6^\circ$ . Surface roughness measurements have been obtained directly on the tool machine and without disassembling the workpiece using a roughness meter (SurfTest 301 Mitutoyo). Concerning cutting forces measurement, the tool holder was mounted on a three-component piezoelectric dynamometer (Kistler 9257B). The measurement chain includes a charge amplifier (Kistler 5019B130), data acquisition hardware (A/D 2855A3) and graphical programming environment (DYNOWARE 2825A1-1) for data analysis and visualization (Fig.1). Material removal rate MRR and power consumption  $P_c$  are calculated using Eq. (1) and Eq. (2) respectively (Sandvik, 2009; Guo et al., 2012).

$$MRR = V_c \cdot a_p \cdot f, \quad (1)$$

$$P_c = (V_c \cdot a_p \cdot f \cdot K_c) / 60, \quad (2)$$

where MRR is in (cm<sup>3</sup>/min) and  $P_c$  in (watt),  $V_c$ ,  $a_p$ ,  $f$  and  $K_c$  are respectively the cutting speed in (m/min), depth of cut in (mm), feed rate in (mm/rev) and specific cutting force in (N/mm<sup>2</sup>).

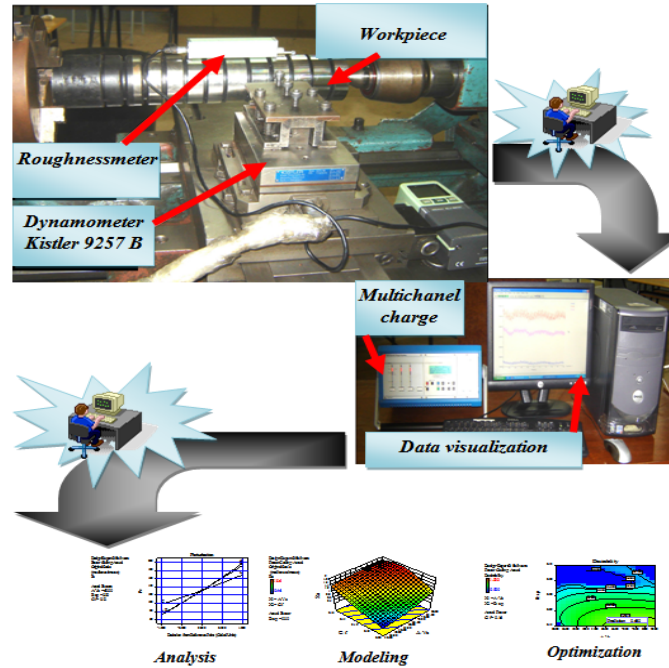


**Fig.1.** Set-up and design of experiments

**2.2. Experimental design**

The experimental approach was carried out in order to investigate the effects of the different factors and their interaction on surface roughness, cutting force components, material removal rate and power consumption. Furthermore, three levels are specified for each factor (Rahman et al. 1997), as shown in Table 1.

**Table 1**

Assignment for the levels to the factors

Level	Cutting speed $V_c$ (m/min)	Feed rate $f$ (mm/rev)	Depth of cut $a_p$ (mm)
-1	30	0.08	0.15
0	60	0.12	0.3
1	90	0.16	0.45

The experimental tests are carried out according to a Box-Behnken design (BBD) with 15 experimental runs composed of three (03) center points. The RSM applied in this work is considered as a procedure to identify a relationship between independent input process parameters and output data (process response). This procedure includes commonly six steps (Gaitonde et al., 2009) : (1) define the independent input variables and the desired output responses, (2) adopt an experimental design plan, (3) perform regression analysis with the required model of RSM as shown in Eq. (3) and Eq. (4) (Hessainia et al., 2013b; Zahia et al., 2015).

$$\Omega = \zeta(v_c, a_p, f, r) + e_{ij}, \tag{3}$$

where,  $\Omega$  presents the desired response and  $\zeta$  denotes the response function. In the procedure of analysis, the approximation of  $\Omega$  was proposed using the fitted second-order polynomial regression model which is called the full quadratic model as follows:

$$\Omega = a_0 + \sum_{i=1}^k a_i X_i + \sum_{i=1}^k a_{ii} X_i^2 + \sum_{i < j}^k a_{ij} X_i X_j , \quad (4)$$

where,  $(a_0)$  is constant,  $(a_i)$ ,  $(a_{ii})$  and  $(a_{ij})$  are the coefficients of linear, quadratic and cross product terms respectively.  $(X_i)$  reveals the coded variables that correspond to the studied machining parameters.

The fellow step (4) is to perform a statistical analysis of variance ANOVA of the independent input variables in order to find parameters which affect the most significantly the response, Eq. (5) determines the situation of the RSM model and decide whether this model needs screening variables or not and finally Eq. (6) optimizes and conducts confirmation experiment with verifying the predicted output parameters. In order to attain this goal of optimization, an objective function  $F(x)$  is defined as follows:

$$F(x) = -DF$$

$$DF = \left( \prod_{i=1}^n d_i^{w_i} \right)^{\frac{1}{\sum_{j=1}^n w_j}}, \quad (5)$$

where  $(d_i)$  is the desirability defined for the  $i^{\text{th}}$  targeted output and  $(w_i)$  is the weighting of  $(d_i)$ . For various goals of each targeted output, the desirability  $(d_i)$  is defined in different forms. If a goal is to reach a specific value of  $(T_i)$ , the desirability  $(d_i)$  is:

$$d_i = 0 \text{ if } Y_i \leq \text{low}_i$$

$$d_i = \left[ \frac{Y_i - \text{low}_i}{T_i - \text{low}_i} \right] \text{ if } \text{low}_i \leq Y_i \leq T_i \quad (6)$$

$$d_i = \left[ \frac{Y_i - \text{High}_i}{T_i - \text{High}_i} \right] \text{ if } T_i \leq Y_i \leq \text{High}_i$$

$$d_i = 0 \text{ if } Y_i \geq \text{High}_i$$

In order to find a maximum, the desirability is shown as follows:

$$d_i = 0 \text{ if } Y_i \leq \text{low}_i$$

$$d_i = \left[ \frac{Y_i - \text{low}_i}{\text{High}_i - \text{low}_i} \right] \text{ if } \text{low}_i \leq Y_i \leq \text{High}_i \quad (7)$$

$$d_i = 1 \text{ if } Y_i \geq \text{High}_i$$

In order to find a minimum, the desirability can be defined by the following formulas:

$$d_i = 1 \text{ if } Y_i \leq \text{low}_i$$

$$d_i = \left[ \frac{\text{High}_i - Y_i}{\text{High}_i - \text{low}_i} \right] \text{ if } \text{low}_i \leq Y_i \leq \text{High}_i \quad (8)$$

$$d_i = 0 \text{ if } Y_i \geq \text{High}_i,$$

where ( $Y_i$ ) is the found value of the  $i^{\text{th}}$  output during optimization processes; ( $low_i$ ) and ( $High_i$ ) are, respectively, the minimum and the maximum values of the experimental data for the  $i^{\text{th}}$  output. In Eq. (3), ( $w_i$ ) are set to one since the ( $d_i$ ) are equally important in this study. The (DF) is a combined desirability function (Myers et al., 2009; Zahia et al., 2015), and the objective is choosing an optimal setting that maximizes a combined desirability function (DF), i.e., minimizes  $F(x)$  (Myers & Montgomery, 2002).

### 3. Results and discussion

The design of experiment was developed for assessing the influence of the cutting speed  $V_c$ , feed rate  $f$  and depth of cut  $ap$  on surface roughness, cutting force, material removal rate MRR and power consumption  $P_c$ . The statistical treatment of the data was made in three phases. The first phase uses ANOVA to study the effect of factors and their interactions. The second phase is associated with the choice of best mobilization to obtain the highest correlation between the parameters using Box-Cox Plot for Power Transforms (Sakia, 1992; Osborne, 2010). Afterwards, in the final phase, the results have to be optimized. It can be shown in Table 2 that the surface roughness  $R_a$  was obtained in the range of (0.46–1.86)  $\mu\text{m}$ . The feed force  $F_a$ , the thrust force  $F_r$  and the tangential force  $F_v$  were obtained in the range of (22.25–101.22) N, (63.56–137.89) N and (53.92–234.88) N, respectively. The material removal rate MRR and power consumption  $P_c$  were obtained, in the range of (0.54–4.86)  $\text{cm}^3/\text{min}$  and (53.92–276.73) Watt respectively.

**Table 2**

Experimental results for surface roughness, cutting force components, material removal rate and power consumption

Run	$V_c$ (m/min)	$ap$ (mm)	$f$ (mm/tr)	$R_a$ ( $\mu\text{m}$ )	$F_a$ (N)	$F_r$ (N)	$F_v$ (N)	MRR ( $\text{cm}^3/\text{min}$ )	$P_c$ (Watt)
1	90	0,45	0,12	1,19	89,27	123,9	184,45	4,86	276,73
2	90	0,3	0,08	1,2	52,92	99,65	97,5	2,16	146,25
3	60	0,3	0,12	1,51	56,17	108,6	129,75	2,16	129,75
4	60	0,3	0,12	1,22	59,33	105,1	132,42	2,16	135,23
5	60	0,3	0,12	1,18	56,17	108,6	129,75	2,16	129,75
6	90	0,3	0,16	1,57	52,55	110,5	167	4,32	250,5
7	30	0,45	0,12	0,8	101,2	135,4	207,93	1,62	103,96
8	30	0,3	0,16	1,5	70,1	130,5	185,75	1,44	92,9
9	30	0,15	0,12	0,54	62,75	98,78	128,24	0,54	64,12
10	60	0,45	0,08	0,47	80,34	109,9	155,11	2,16	155,11
11	90	0,15	0,12	1,41	24,88	73,74	75	1,62	112,5
12	60	0,15	0,08	0,58	22,25	63,56	53,92	0,72	53,92
13	60	0,45	0,16	1,86	91,24	137,8	234,88	4,32	234,88
14	30	0,3	0,08	0,46	56,06	93,98	126	0,72	63
15	60	0,15	0,16	0,88	26,91	87,45	98,94	1,44	98,94

#### 3.1. Statistical analysis

A variance analysis of the surface roughness, cutting force components, material removal rate and power consumption were performed with the objective of analyzing the influence of cutting speed, feed rate, depth of cut on the obtained outputs. Table 3, Table 4 (a, b and c), Table 5 and Table 6 show the results of ANOVA for  $R_a$ ,  $F_a$ ,  $F_r$ ,  $F_v$ , MRR and  $P_c$ , respectively. This analysis was carried out for a 5% significance level, i.e., for a 95% confidence level.

##### 3.1.1. Surface roughness

According to Table 3, it can be observed that the significant terms on roughness  $R_a$  were  $V_c$ ,  $ap$  and  $f$ , the product  $V_c*ap$ ,  $V_c*f$ ,  $ap*f$  and the squares  $ap^2$  and  $f^2$ . The perturbation plot in Fig. 2 helps to compare the effect of all the factors at a particular point in the design space. A steep slope for  $V_c$  and  $f$  or curvature in a factor  $ap$  shows that the response is sensitive to those factors. Indeed, from Table 3 that shows ANOVA for  $R_a$ , it can be seen that the most significant factor on the parameters  $R_a$  was the feed rate  $f$ ,

which explains, 43.58% contributions of the total variation. The next largest contribution on  $Ra$  comes from the cutting speed  $Vc$  with the contributions of 23.85 %. Depth of cut  $ap$  have the lowest contribution value of contribution ratio (1.67 %), which confirms results of Ramanujam et al. (2014). Indeed, they did not present a statistical significance on surface roughness parameter. In addition, it is clearly observed that the feed rate  $f$  strongly affects surface roughness parameter  $Ra$ . This input parameter has an increasing effect that should be expected. It is well known that the theoretical geometrical surface roughness is primarily a function of the feed rate for a given nose radius and varies with the square of the feed rate value. This is in good agreement with the established following equation (Zahia et al., 2013a; Davim et al., 2008).

$$Ra = \frac{f^2}{32 \cdot r_\epsilon}, \quad (9)$$

where  $f$  is the feed rate in (mm/rev) and  $r_\epsilon$  is the nose radius of the tool in (mm).

**Table 3**  
Analysis of variance for  $Ra$ .

Source	Sum of Squares	df	Mean Square	F Value	P-value	Cont %
Model	0,875406	9	0,097267	47,55736	0.0003	98,85
$Vc$	0,21124	1	0,21124	103,2826	0.0002	23,85
$ap$	0,014751	1	0,014751	7,212088	0.0435	1,67
$f$	0,385922	1	0,385922	188,6907	< 0.0001	43,58
$Vc*ap$	0,025176	1	0,025176	12,30952	0.0171	2,84
$Vc*f$	0,07375	1	0,07375	36,05892	0.0018	8,33
$ap*f$	0,054392	1	0,054392	26,59422	0.0036	6,14
$Vc^2$	0,000608	1	0,000608	0,297189	0.6091	0,07
$ap^2$	0,085445	1	0,085445	41,77687	0.0013	9,65
$f^2$	0,032047	1	0,032047	15,66881	0.0108	3,62
Residual	0,010226	5	0,002045			1,15
Lack of Fit	0,008059	3	0,002686	2,478984	0.3004	0,91
Pure Error	0,002167	2	0,001084			0,24
Cor Total	0,885632	14				100,00

In addition, high feed rate causes high tool nose displacement and amplitude vibration. This can degraded surface workpiece state by increasing surface roughness criteria  $Ra$ , this can be confirmed by results reported by (Zahia et al., 2013a), in turning roughness model based on tool-nose displacements. The cutting speed effect has less importance (Ramanujam et al., 2014). Surface roughness was higher by increasing cutting speed (Thakur et al., 2009), producing a poor surface finish at higher cutting speed. In addition, the increasing of cutting speed increases the MRR, the increasing of MRR causes an increasing of material quantity ahead the nose. However, we have a high built up edge formation probability and poor surface finish quality.

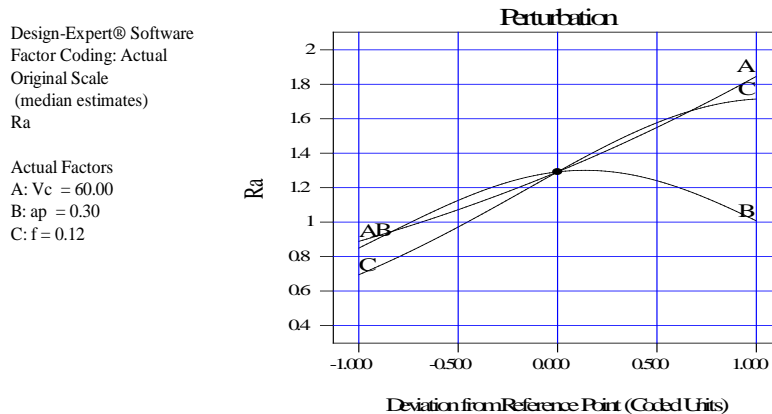
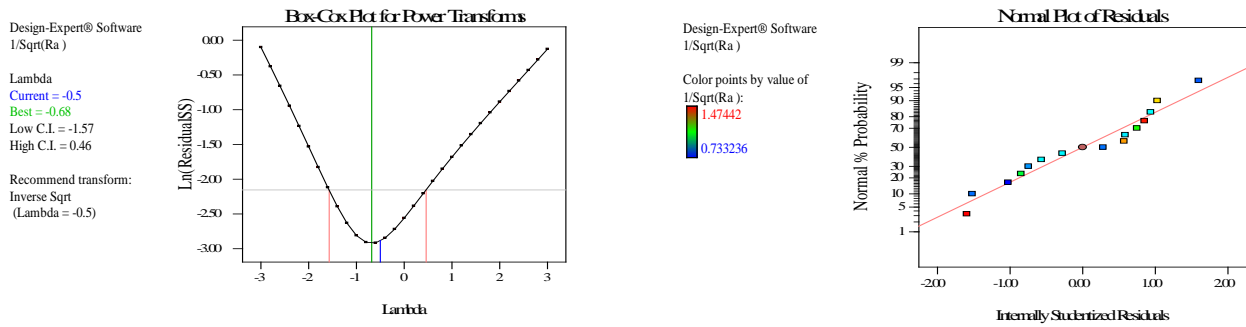


**Fig. 2.** Perturbation plot for  $Ra$

Fig. 3 (a) shows the Box-Cox plot for  $Ra$ . This plot provides a guideline for selecting the correct power law transformation (Sakia, 1992; Osborne, 2010). A recommended transformation is listed, based on the best lambda value, which is found at the minimum point of the curve generated by the natural log of the sum of squares of the residuals. From this figure we can see that the current  $\lambda$  value for the chosen law transformation is (-0.5) and its recommended value is (-0.5). For this the chosen law transformation is shown in Eq. (10).

$$[Ra]^{\lambda} = \frac{1}{\sqrt{Ra}} = a_0 + \sum_{i=1}^3 a_i X_i + \sum_{i=1}^3 a_{ii} X_i^2 \tag{10}$$



(a) (b)  
**Fig. 3.** Box-Cox plot (a) and normal plot of residuals (b) for  $Ra$

The normal plot of residuals for the surface roughness criteria ( $Ra$ ) was presented in Fig. 3 (b). The data follows the straight line (Sahoo & Mishra, 2014), closely. This indicates that a transformation of the response provides a better analysis, and the models proposed in Eq. (10) are adequate.

3.1.2. Cutting force components

Table 4(a), (b) and (c) show ANOVA results corresponding to the cutting force components. These tables show that the effects of cutting speed  $V_c$  and depth of cut  $ap$  are all significant with respect to the thrust, feed and tangential cutting forces. The effects of the square  $V_c^2$  are significant with respect to the tangential cutting forces. Likewise, it can be realized that the product  $V_c * f$  and feed rate  $f$ , have statistical significance on the thrust cutting force.

The perturbation plot in Fig. 4 indicates that the cutting force components ( $F_a$ ,  $F_r$  and  $F_v$ ) are significantly affected by depth of cut and cutting speed. A relatively flat line in feed rate  $f$  shows insensitivity to change in that particular factor in term of feed force  $F_a$  (Fig. 4(a)). These graphs show that the cutting force components also increase when the feed rate and the depth of cut increase. Because the depth of cut and the feed rate increases, the tool-chip interface area and chip section should be increased, which lead to increase in cutting force components. The depth of cut has maximum influence on the cutting force components:  $F_a$ ,  $F_r$  and  $F_v$  with the contributions of: 79.87%, 66.92% and 66.26%, respectively, followed by feed rate (1.34%, 19.69% and 23.54%) and cutting speed (7.82%, 5.05 % and 5.60%).

The cutting speed has decreasing control on cutting forces components ( $F_a$ ,  $F_r$  and  $F_v$ ) (Choudhury & El-Baradie, 1999). The increase in cutting speed leads to enhance temperature and consequently the softening of the workpiece material. Therefore, the cutting force shows a decreasing trend. However, the effect of cutting speed on cutting forces was significant for cutting speeds of (30-90) m/min.

Fig. 5 (a), Fig. 6 (a) and Fig. 7 (a), show the Box-Cox plots for  $F_a$ ,  $F_r$  and  $F_v$ . From this figure the current  $\lambda$  values for the law transformation for  $F_a$ ,  $F_r$  and  $F_v$  are (1.0, 1.0 and 1.0), respectively

according to recommended values. Thus, the chosen law transformations for  $Fa$ ,  $Fr$  and  $Fv$  are shown in Eq. (11), Eq. (12) and Eq. (13) respectively (Sakia, 1992; Osborne, 2010).

$$[Fa]^{lamda} = [Fa]^{1.0} = a_0 + \sum_{i=1}^3 a_i X_i + \sum_{i=1}^3 a_{ii} X_i^2 + \sum_{i<j}^3 a_{ij} X_i X_j \quad (11)$$

$$[Fr]^{lamda} = [Fr]^{1.0} = a_0 + \sum_{i=1}^3 a_i X_i + \sum_{i=1}^3 a_{ii} X_i^2 + \sum_{i<j}^3 a_{ij} X_i X_j \quad (12)$$

$$[Fv]^{lamda} = [Fv]^{1.0} = a_0 + \sum_{i=1}^3 a_i X_i + \sum_{i=1}^3 a_{ii} X_i^2 + \sum_{i<j}^3 a_{ij} X_i X_j \quad (13)$$

**Table 4**

Analysis of variance for  $Fa$ ,  $Fr$  and  $Fv$

(a) Analysis of variance for $Fa$						
Source	Sum of Squares	df	Mean Square	F Value	P-value	Cont %
Model	7779,265	9	864,3628	26,51179	0.0011	97,95
Vc	621,45751	1	621,4575	19,06138	0.0072	7,82
ap	6343,8848	1	6343,885	194,58	< 0.0001	79,87
f	106,79911	1	106,7991	3,275749	0.1301	1,34
Vc*ap	167,9616	1	167,9616	5,151729	0.0725	2,11
Vc*f	51,912025	1	51,91203	1,592249	0.2627	0,65
ap*f	9,7344	1	9,7344	0,298574	0.6083	0,12
Vc <sup>2</sup>	173,73742	1	173,7374	5,328885	0.0690	2,19
ap <sup>2</sup>	63,195539	1	63,19554	1,938338	0.2226	0,80
f <sup>2</sup>	206,8854	1	206,8854	6,345602	0.0532	2,60
Residual	163,01479	5	32,60296			2,05
Lack of Fit	154,34033	3	51,44678	11,86166	0.0787	1,94
Pure Error	8,6744667	2	4,337233			0,11
Cor Total	7942,2798	14				100,00
(b) Analysis of variance for $Fr$ .						
Source	Sum of Squares	df	Mean Square	F Value	P-value	Cont %
Model	6205,974	9	689,5527	35,73352	0.0005	98,47
Vc	318,0242	1	318,0242	16,48043	0.0097	5,05
ap	4217,293	1	4217,293	218,5456	< 0.0001	66,92
f	1241,016	1	1241,016	64,31108	0.0005	19,69
Vc*ap	46,30803	1	46,30803	2,399742	0.1820	0,73
Vc*f	160,149	1	160,149	8,299131	0.0346	2,54
ap*f	3,940225	1	3,940225	0,204188	0.6703	0,06
Vc <sup>2</sup>	69,88108	1	69,88108	3,621328	0.1154	1,11
ap <sup>2</sup>	81,02888	1	81,02888	4,199022	0.0957	1,29
f <sup>2</sup>	55,8604	1	55,8604	2,894759	0.1496	0,89
Residual	96,48542	5	19,29708			1,53
Lack of Fit	77,75135	3	25,91712	2,766844	0.2766	1,23
Pure Error	18,73407	2	9,367033			0,30
Cor Total	6302,46	14				100,00
(c) Analysis of variance for $Fv$						
Source	Sum of Squares	df	Mean Square	F Value	P-value	Cont %
Model	33874,43	9	3763,825	45,59985	0.0003	98,80
Vc	1921,07	1	1921,07	23,27433	0.0048	5,60
ap	22717,53	1	22717,53	275,2295	< 0.0001	66,26
f	8069,581	1	8069,581	97,76533	0.0002	23,54
Vc*ap	222,01	1	222,01	2,689716	0.1619	0,65
Vc*f	23,57103	1	23,57103	0,28557	0.6160	0,07
ap*f	301,8906	1	301,8906	3,657493	0.1140	0,88
Vc <sup>2</sup>	568,7217	1	568,7217	6,890229	0.0468	1,66
ap <sup>2</sup>	60,588	1	60,588	0,734041	0.4307	0,18
f <sup>2</sup>	2,314103	1	2,314103	0,028036	0.8736	0,01
Residual	412,7015	5	82,54031			1,20
Lack of Fit	397,9031	3	132,6344	17,92542	0.0533	1,16
Pure Error	14,79847	2	7,399233			0,04
Cor Total	34287,13	14				100,00

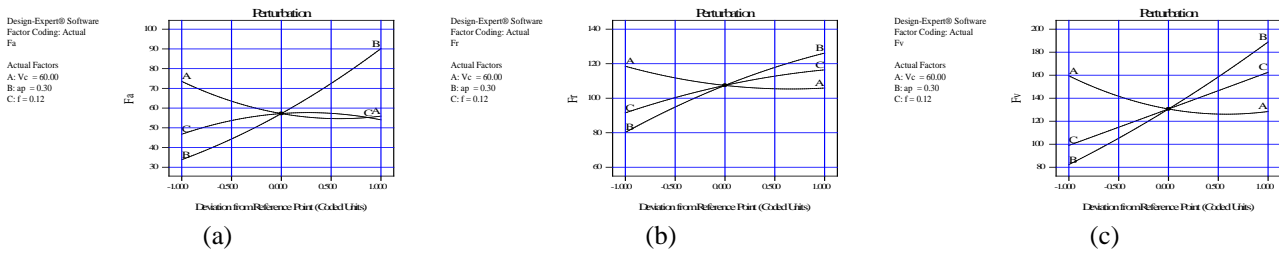


Fig. 4. Perturbation plot for  $F_a$  (a),  $F_r$ (b) and  $F_v$  (c)

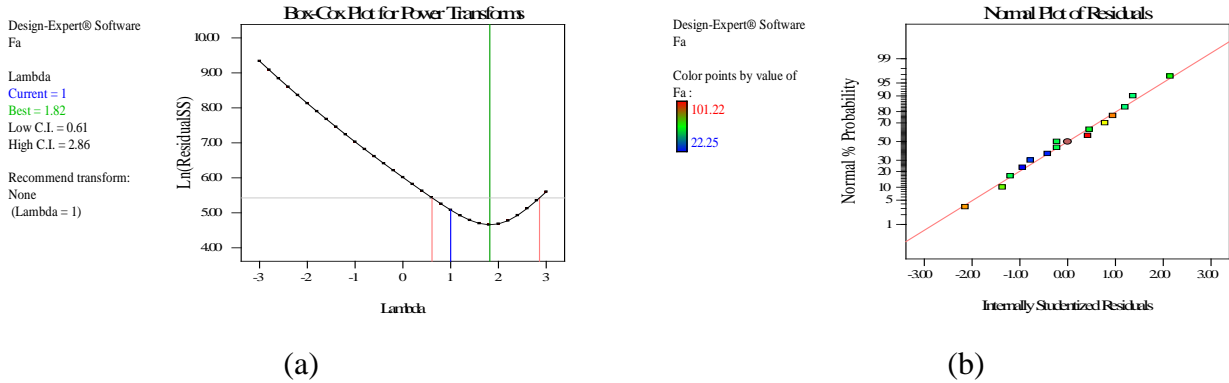


Fig. 5. Box-Cox plot (a) and normal plot of residuals (b) for  $F_a$

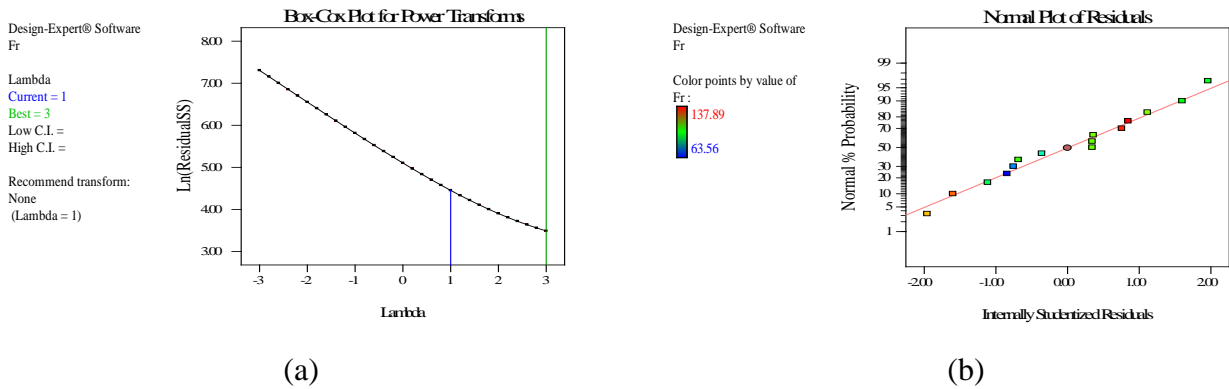


Fig. 6. Box-Cox plot (a) and normal plot of residuals (b) for  $F_r$

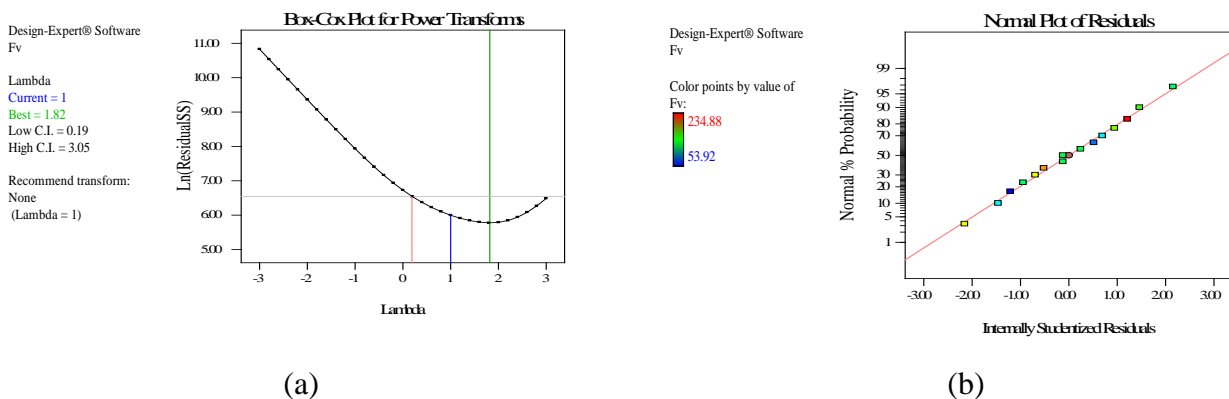


Fig.7. Box-Cox plot (a) and normal plot of residuals (b) for  $F_v$

Normal plots of residuals for the cutting force components  $F_a$ ,  $F_r$  and  $F_v$  can be observed in Fig. 5 (b), Fig. 6 (b) and Fig. 7 (b). Data follows the straight line, closely. This indicates that the transformation of the response for each component provides a good analysis, and the models proposed in Eq. (11), Eq. (12) and Eq. (13) are adequate (Sahoo & Mishra, 2014).

3.1.3. Material removal rate

The Table 5 shows ANOVA associated with the material removal rate MRR. This table shows that the effects of cutting speed, depth of cut  $ap$ , feed rate  $f$  and the products  $Vc*ap$ ,  $Vc*f$  and  $ap*f$  are all significant.

The perturbation plot in Fig. 8 shows a steep slope for cutting  $Vc$  and depth of cut  $ap$  comparing with feed rate  $f$ , consequently, the response is sensitive to these factors. Indeed, from Table 5, it can be seen that the  $Vc$ ,  $ap$ ,  $f$ ,  $Vc*ap$ ,  $Vc*f$  and  $ap*f$  having contributions values of (37.31%), (37.31%), (16.58%), (4.66%), (2.07%) and (2.07%) respectively.

Material removal rate is calculated using Eq. (1), for this we have not residuals (Fig. 9). Consequently, the chosen  $lambda$  value for the law transformation for  $MRR$  is (1.0) as shown in Eq. (14) (Sakia, 1992; Osborne, 2010).

$$[MRR]^{lambda} = [MRR]^{1.0} = a_0 + \sum_{i=1}^3 a_i X_i + \sum_{i=1}^3 a_{ii} X_i^2 + \sum_{i<j}^3 a_{ij} X_i X_j \tag{14}$$

**Table 5**  
Analysis of variance for MRR

Source	Sum of Squares	df	Mean Square	F Value	P-value	Cont %
Model	25,0128	9	2,7792	63660000	< 0.0001	100,00
Vc	9,3312	1	9,3312	63660000	< 0.0001	37,31
ap	9,3312	1	9,3312	63660000	< 0.0001	37,31
f	4,1472	1	4,1472	63660000	< 0.0001	16,58
Vc*ap	1,1664	1	1,1664	63660000	< 0.0001	4,66
Vc*f	0,5184	1	0,5184	63660000	< 0.0001	2,07
ap*f	0,5184	1	0,5184	63660000	< 0.0001	2,07
Vc <sup>2</sup>	0	1	0			0,00
ap <sup>2</sup>	0	1	0			0,00
f <sup>2</sup>	0	1	0			0,00
Residual	0	5	0			0,00
Lack of Fit	0	3	0			0,00
Pure Error	0	2	0			0,00
Cor Total	25,0128	14				100,00

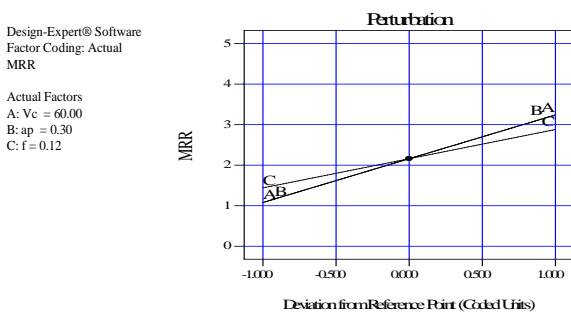


**Fig. 8.** Perturbation plot for MRR

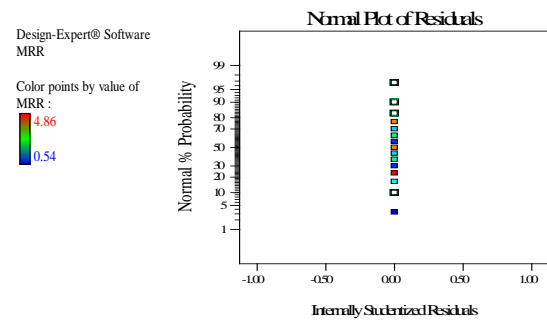


**Fig. 9.** Normal plot of residuals for MRR

3.1.4. Power consumption

Table 6 shows the results of ANOVA corresponding to the power consumption. This table shows that the cutting speed  $Vc$ , depth of cut  $ap$ , feed rate  $f$  and the products  $Vc *ap$ ,  $Vc*f$ ,  $ap*f$ , the square term  $Vc^2$  and  $ap^2$  are all significant on  $Pc$ , with contributions values of 38,35%, 34,32% , 12,35%, 9,03%, 3,60%, 1,34% ,0,62%, 0,32%, respectively. The perturbation plot for the power consumption  $Pc$  are presented in Fig. 10, a steep slope in a factors shows that the response is significantly affected by feed rate, depth of cut and cutting speed.

**Table 6**  
Analysis of variance for Pc

Source	Sum of Squares	df	Mean Square	F Value	P-value	Cont %
Model	53156394,3	9	5906266,03	573,274838	< 0.0001	99,90
Vc	20402911,7	1	20402911,7	1980,35034	< 0.0001	38,35
ap	18262514,5	1	18262514,5	1772,5988	< 0.0001	34,32
f	6569568,99	1	6569568,99	637,656445	< 0.0001	12,35
Vc*ap	4802517,91	1	4802517,91	466,14268	< 0.0001	9,03
Vc*f	1914814,81	1	1914814,81	185,856029	< 0.0001	3,60
ap*f	715026,04	1	715026,04	69,4019598	0.0004	1,34
Vc <sup>2</sup>	329308,882	1	329308,882	31,9634258	0.0024	0,62
ap <sup>2</sup>	170270,391	1	170270,391	16,5268091	0.0097	0,32
f <sup>2</sup>	49161,7528	1	49161,7528	4,77174508	0.0807	0,09
Residual	51513,3897	5	10302,6779			0,10
Lack of Fit	41935,9122	3	13978,6374	2,91906452	0.2655	0,08
Pure Error	9577,47752	2	4788,73876			0,02
Cor Total	53207907,7	14				100,00

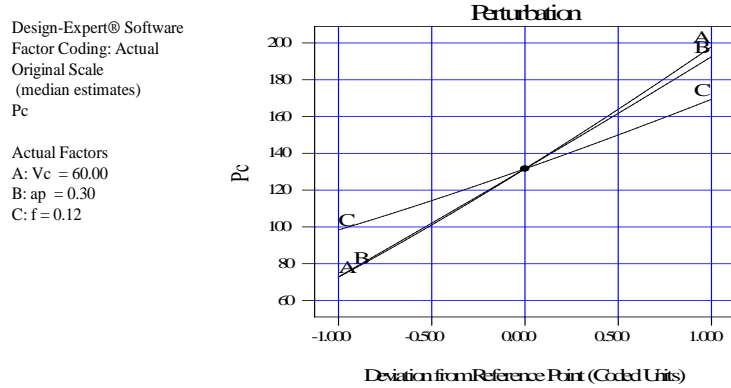


**Fig. 10.** Perturbation plot for Pc

Fig. 11 (a) shows the Box-Cox plots and for Pc. From this figure we can see that the current *lambda* value for the chosen law transformation for Pc is (1.57) and its recommended value is (1.57) (Sakia, 1992; Osborne, 2010). For this, the law transformation for response is shown in Eq. (15).

$$[Pc]^{lambda} = [Pc]^{1.57} = a_0 + \sum_{i=1}^3 a_i X_i + \sum_{i=1}^3 a_{ii} X_i^2 + \sum_{i < j}^3 a_{ij} X_i X_j \tag{15}$$

The normal plot of residuals for the power consumption Pc was plotted in Fig. 11 (b). The data follows the straight line, closely. This indicates that a transformation of the response for each component provides a better analysis, and the model proposed in Eq. (15) is adequate (Sahoo & Mishra, 2014).

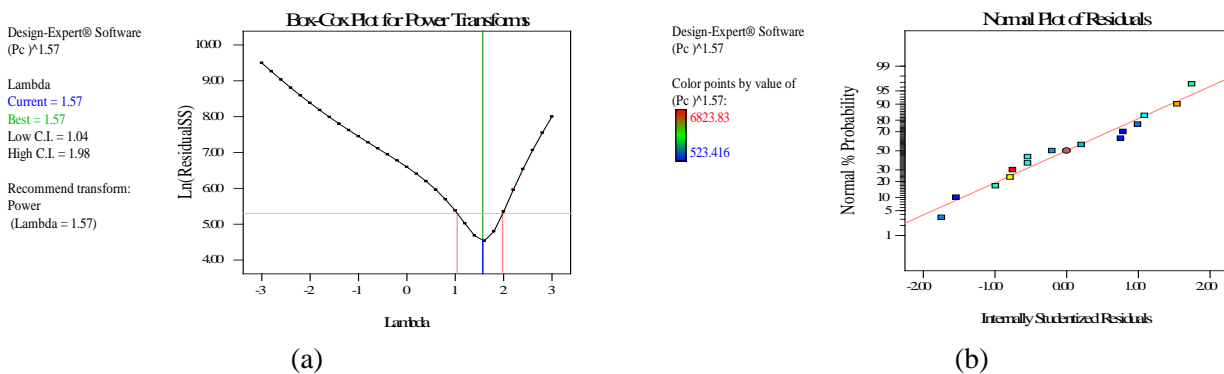


**Fig. 11.** Box-Cox plot (a) and normal plot of residuals (b) for Pc

### 3.2. Mathematical models

The initial analysis of the responses obtained from RSM includes all parameters and their interactions. The relationship between the factors and the performance measures were modeled by full quadratic regression. Based on Eq. (10), Eq. (11), Eq. (12), Eq. (13), Eq. (14) and Eq. (15), the roughness  $Ra$ , feed force  $Fa$ , thrust force  $Fr$ , tangential force  $Fv$ , material removal rate MRR and power consumption  $Pc$  models are given below in Eq. (16), Eq. (17), Eq. (18), Eq. (19), Eq. (20) and Eq. (21), respectively.

$$Ra (\mu\text{m}) = \frac{1}{\left( \begin{aligned} &(3.894921 - 0.02599(Vc) - 3.06845(ap) - 20.4241(f) + 0,01763(Vc * ap) + 0.113154(Vc * f) - \\ &19.4351(ap * f) + 43E - 05 (Vc^2) + 6.761003(ap^2) + 58.2269 (f^2) \end{aligned} \right)^2} \quad (16)$$

$$R^2 = 0.988, \text{Adj } R^2 = 0.967$$

$$Fa (N) = -0.8375 - 1.28015(Vc) - 40.1888(ap) + 1316.28125(f) + 1.44(Vc * ap) - 3.0020(Vc * f) + 260(ap * f) + 0.00762(Vc^2) + 183.87037(ap^2) - 4678.38542 (f^2) \quad (17)$$

$$R^2 = 0.979 \text{ Adj } R^2 = 0.942$$

$$Fr (N) = -17.1112 - 0.3843(Vc) + 212.7722(ap) + 1161.5625(f) + 0.7561(Vc * ap) - 5.2729(Vc * f) + 165.4166(ap * f) + 0.0048(Vc^2) - 208.2037(ap^2) - 42430.9895 (f^2) \quad (18)$$

$$R^2 = 0.979 \text{ Adj } R^2 = 0.942$$

$$Fv (N) = 116.8 - 2.9107(Vc) - 25.8472(ap) + 357(f) + 1.6555(Vc * ap) + 2.0229(Vc * f) + 1447.91(ap * f) + 0.0137(Vc^2) + 180.0370(ap^2) - 494.7916 (f^2) \quad (19)$$

$$R^2 = 0.987, \text{Adj } R^2 = 0.966$$

$$\text{MRR (cm}^3/\text{min)} = 2.16 - 0.036(Vc) - 7.2(ap) - 18(f) + 1.44(Vc * ap) + 0.12(Vc * f) + 60(ap * f) + 1.0931E - 18(Vc^2) + 5.1504E - 14(ap^2) - 6.7191E - 13 (f^2) \quad (20)$$

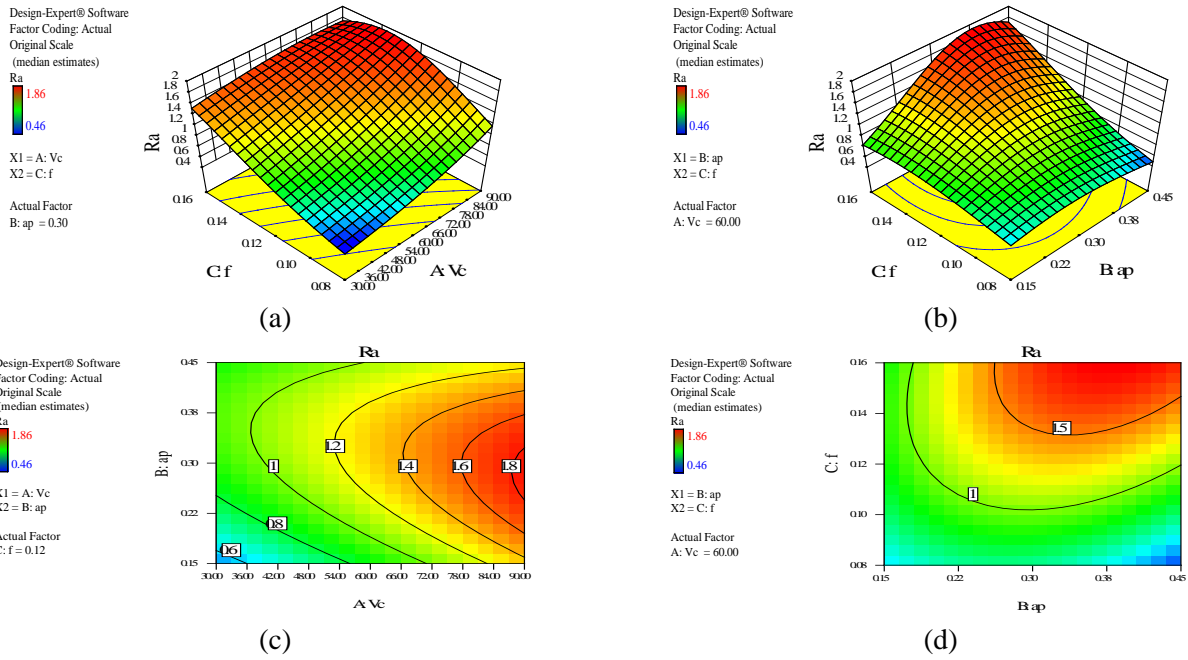
$$R^2 = 1, \text{Adj } R^2 = 1$$

$$Pc(\text{Watt}) = \left[ \begin{aligned} &7375.0107 - 128.8234(Vc) - 18719.5309(ap) - 50387.4065(f) + 243.4960(Vc * ap) + \\ &576.5701(Vc * f) + 70466.0103(ap * f) + 0.331825(Vc^2) + 9544.1686(ap^2) + 72118.1793(f^2) \end{aligned} \right]^{\frac{1}{1.57}} \quad (21)$$

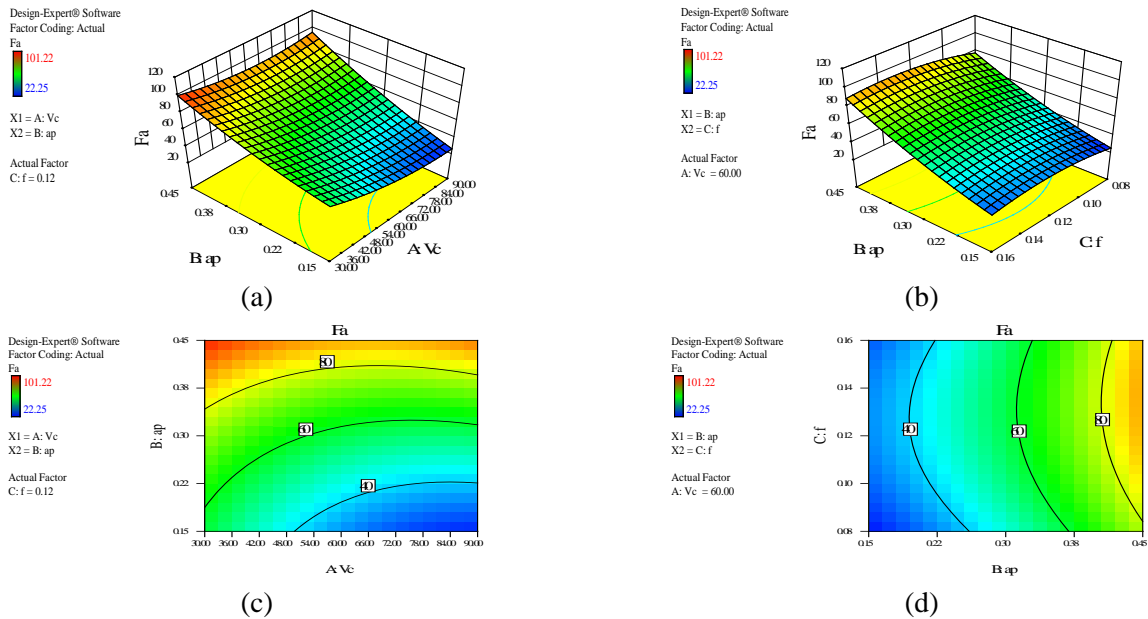
$$R^2 = 0.999, \text{Adj } R^2 = 0.997$$

Based on model shown in Eq. (16) and from Figs. 12 (a), (b), (c) and (d) and contour plot for  $Ra$ , it can be seen that for low depth of cut, the surface roughness was highly sensitive to feed rate. An increase in the latter sharply degrades the surface finish. Nevertheless, this increase yields the smallest with the lowest values of depth of cut which usually does not have much influence on the surface roughness. In addition, it was revealed that a combination of lower cutting speed along with lower feed rate and depth of cut was necessary for obtaining better surface finish (Choudhury & El-Baradie, 1999).

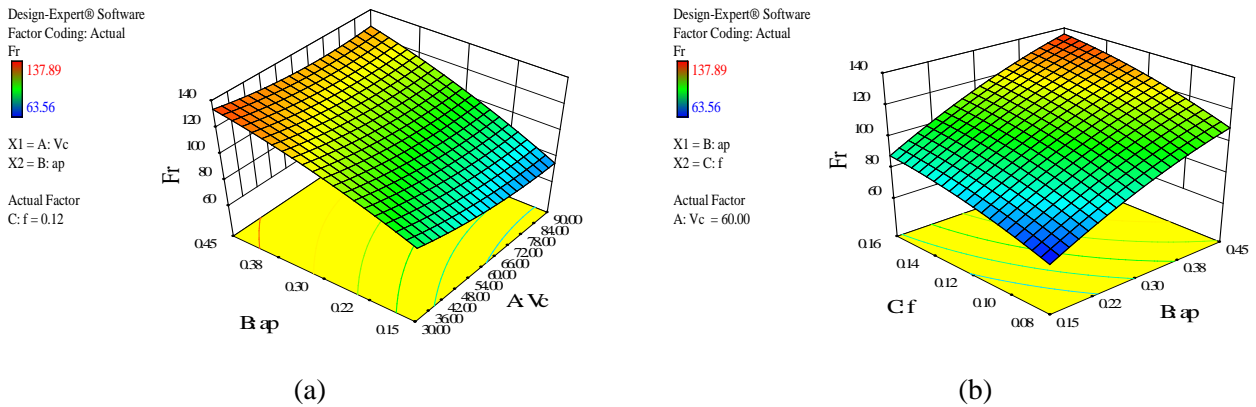
Concerning cutting forces, as seen from the 3D surface plots in Figs. (13-14), Fig. 15(a) and Fig. (b) and contour plots in Figs. (13-14), Fig. 15(c) and Fig. 15(d), that for a given cutting speed, the feed force, thrust force and tangential force sharply increases with the increase in depth of cut or feed rate. The component forces  $Fa$ ,  $Fr$  and  $Fv$  are highly sensitive to depth of cut, as shown in Fig. (13-14) and Fig. 15(c) and Fig. (d). From the above discussions and based on the models shown in Eq. (17), Eq. (18) and Eq. (19), it can be manifest that the cutting forces can be minimized by employing lower values of both feed rate  $f$  and  $ap$  and at highest value of cutting speed  $Vc$ . Also it can be underlined that tangential component  $Fv$  is usually the largest force among the other ones. The thrust component  $Fr$  is the middle force and feed force  $Fa$  is the smallest one (Thakur et al., 2009; Pawade et al., 2007). For the material removal rate MRR, based on the Eq. (20) it can be seen from Figs. 16 (a-d), that the highest MRR can be resulted by combination of highest  $Vc$ , higher value of  $ap$  and higher value of  $f$ . In addition, the lowest MRR value can be observed at lower values of  $Vc$ ,  $ap$  and  $f$ . For the power consumption  $Pc$ , it has been revealed that a combination of the highest cutting speed along with higher feed rate and depth of cut led to maximize  $Pc$  necessary for machining.

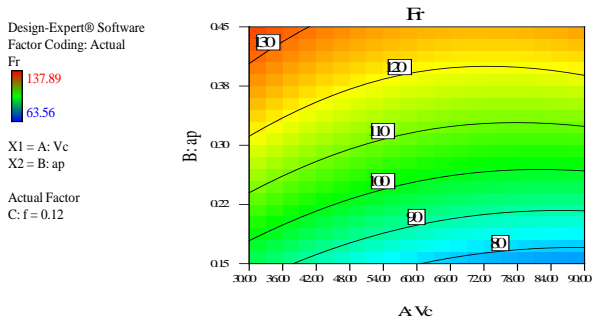


**Fig. 12.** 3D surface plot (a), (b) and Contour Plot (c), (d) for Ra

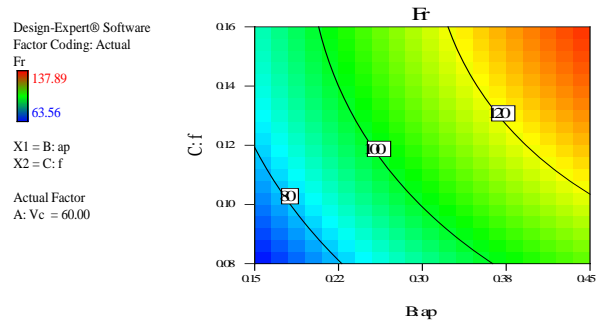


**Fig. 13.** 3D surface plot (a), (b) and Contour Plot (c), (d) for Fa



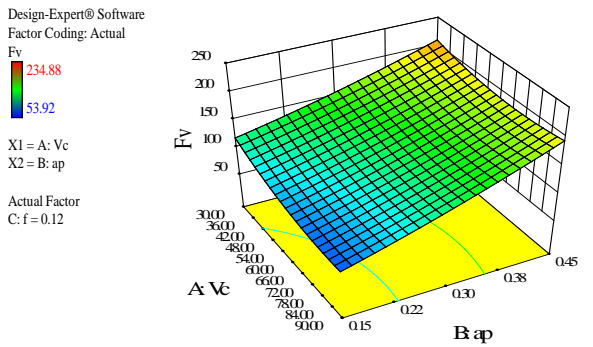


(c)

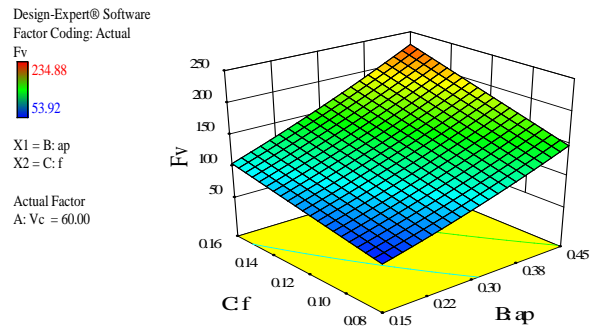


(d)

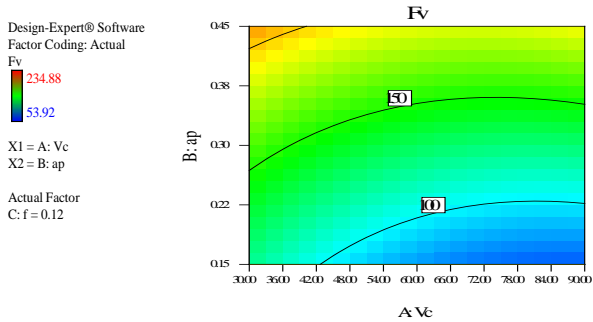
**Fig. 14.** 3D surface plot (a), (b) and Contour Plot (c), (d) for Fr



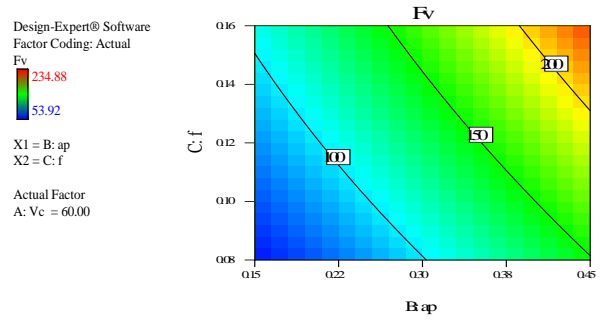
(a)



(b)

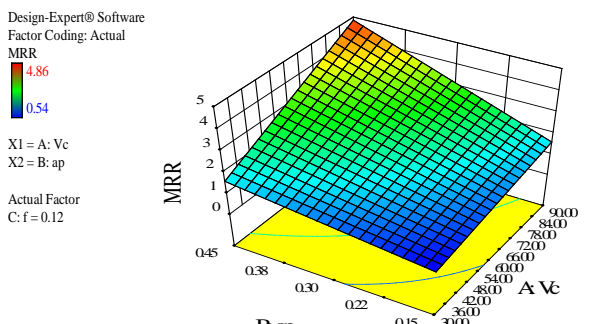


(c)

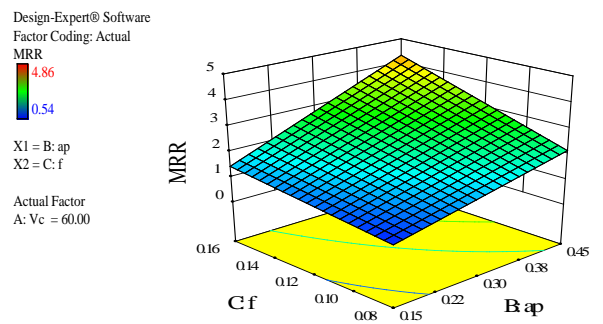


(d)

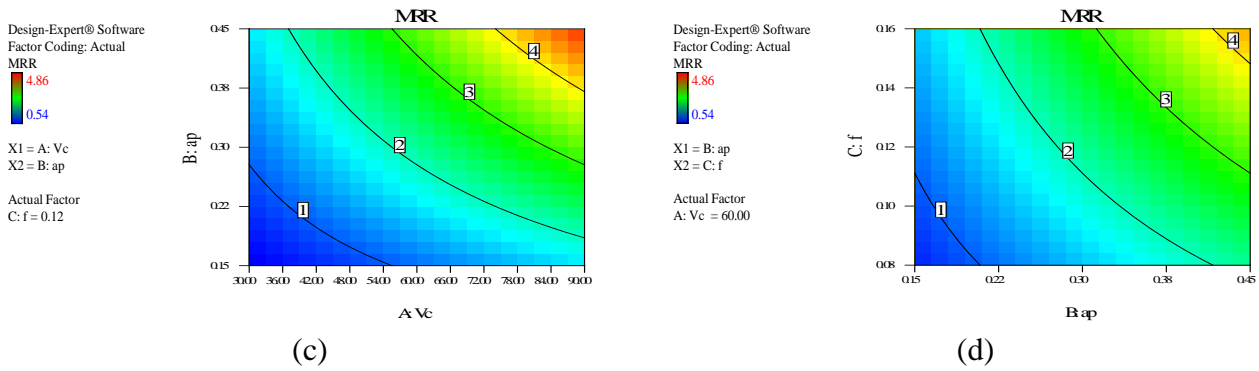
**Fig. 15.** 3D surface plot (a), (b) and Contour Plot (c), (d) for Fv



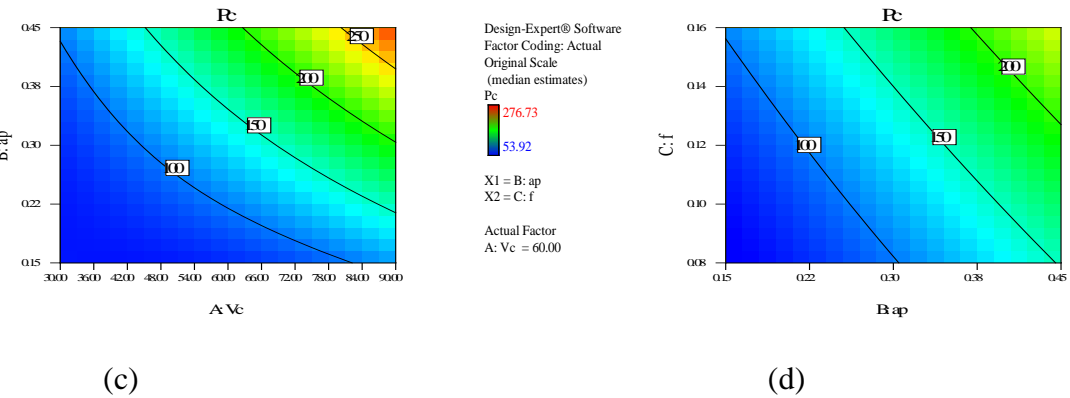
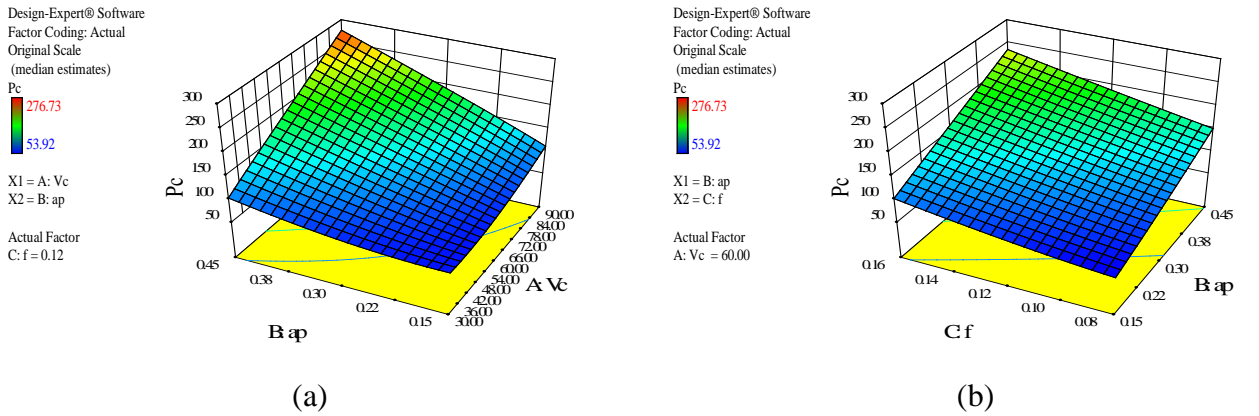
(a)



(b)

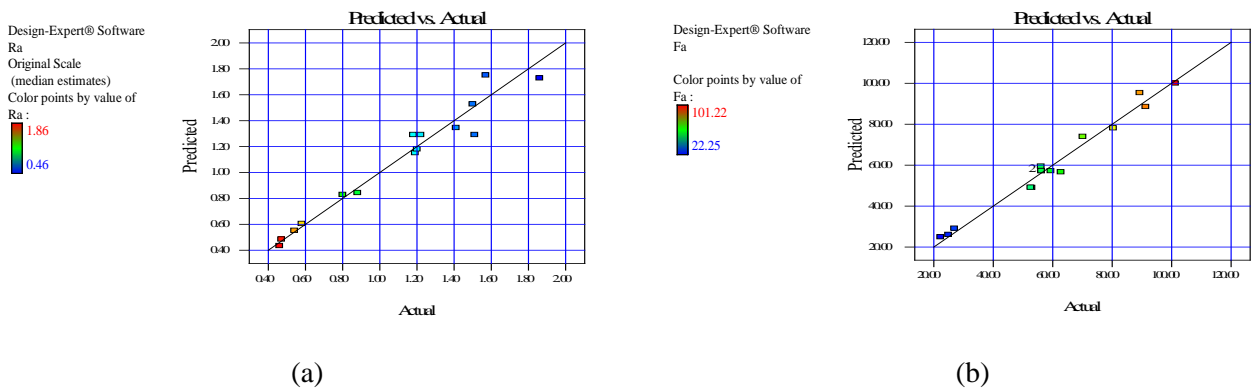


**Fig. 16.** 3D surface plot (a), (b) and Contour Plot (c), (d) for MRR



**Fig. 17.** 3D surface plot (a), (b) and Contour Plot (c), (d) for Pc

The comparison between experimental and predicted response for  $R_a$ ,  $F_a$ ,  $F_r$ ,  $F_v$ ,  $MRR$  and  $P_c$  were illustrated in Fig. 18(a), Fig. 18(b), Fig.18(c), Fig. 18(d), Fig. 18(e) and Fig. 18(f), respectively.



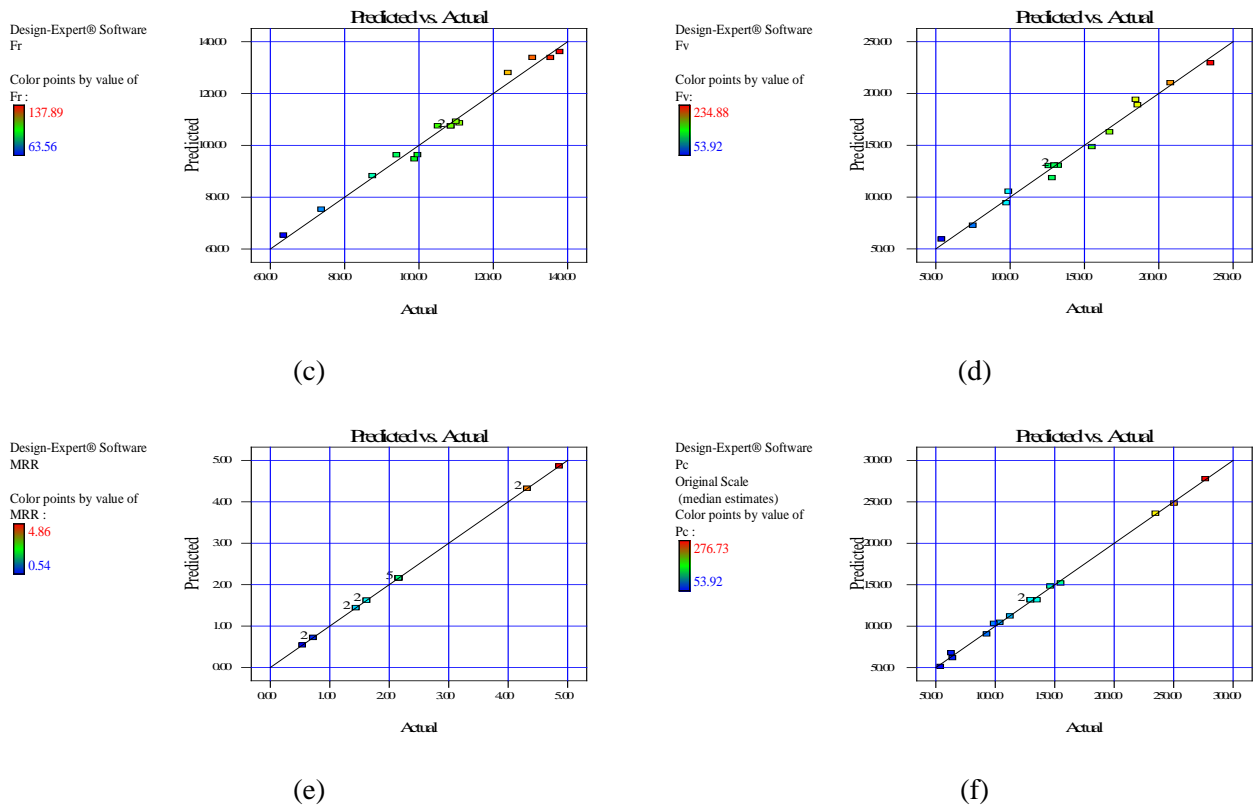


**Fig. 18.** Comparison between actual and predicted values for  $Ra$  (a),  $Fa$  (b),  $Fr$  (c),  $Fv$  (d),  $MRR$  (e) and  $Pc$  (f)

The results of comparison were proven to predict the surface roughness parameter, cutting force, material removal rate and power consumption close to those readings recorded experimentally with a 95% confidence interval. According to this figure, it can be seen that points split is evenly by the 45 degree line. This reflects a good agreement between actual values illustrated in Table 2 and predicted values obtained with models shown in Eq. (16-21).

### 3.3. Response optimization

One of the main goals for the experiment is to investigate the optimal values of cutting parameters in order to obtain the desired value of the machined surface roughness (better roughness  $Ra$ ), the lowest cutting force components ( $Fa$ ,  $Fr$  and  $Fv$ ) and greater material removal rate using minimal power during turning process using different importance degrees for each output parameter (Table 7). The use of response surface optimization helps to identify the combination of input variable settings ( $Vc$ ,  $ap$  and  $f$ ) that jointly optimize the surface roughness value, cutting force components, material removal rate and power consumption during turning process (Hessainia et al., 2013b; Zahia et al., 2015).

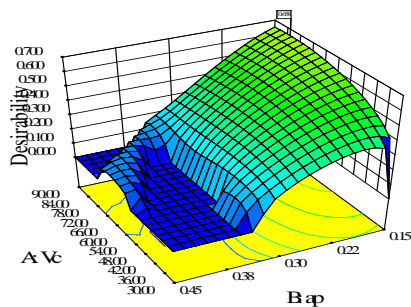
Joint optimization should satisfy the requirements for all the responses in the set. The optimization success is measured by the composite desirability which is weighted from zero to one. Value of 1.0 represents the ideal case and zero indicates that one or more responses are outside acceptable limits (Myers et al., 2009). Table 7 (a, b and c), show the goals, parameter ranges and importance degrees for the output parameters for three cases. The optimum cutting parameters obtained for case (1), with the importance degrees of 3 for  $Ra$ ,  $Fa$ ,  $Fr$ ,  $Fv$ ,  $MRR$  and  $Pc$  are chosen in terms of the highest desirability value (Fig. 19 (a) and (b)) with cutting speed of 85.26 m/min, feed rate of 0.16 mm/rev and cutting depth of 0.15 mm. The predicted responses are  $Ra = 0.97 \mu\text{m}$ ,  $Fa = 18,53 \text{ N}$ ,  $Fr = 78,12 \text{ N}$ ,  $Fv = 97,66 \text{ N}$ ,  $2.19 \text{ cm}^3/\text{min}$  for  $MRR$  and  $152.33 \text{ Watt}$  for  $Pc$ , with desirability value of 0.66 chosen according to Eq. (7) as shown in Fig. 20 which presents solution ramps of multi-objective optimization for case (1) (Hessainia et al., 2013b; Zahia et al., 2015).

Concerning the second case, the importance degrees are chosen as 5 for Ra and 2 for MRR as shown in Table 7 (b). Optimal solution is selected according to maximal desirability value (Fig. 21 (a) and (b)) to be cutting speed of 90.00 m/min, feed rate of 0.08 mm/rev and cutting depth of 0.45 mm. The predicted responses are Ra = 0.65µm and 3.42 cm<sup>3</sup>/min for MRR with desirability value of 0.78 which is chosen according to Eq. (7) as shown in Fig. 22, which presents a solution ramps of multi-objective optimization for case (2). For the third case, the importance degree is chosen as 5 for Ra. Optimal solution is selected according to maximal desirability value cited in Eq. (7) (Fig. 23 (a) and (b)) to be cutting speed of 49.18 m/min, feed rate of 0.08 mm/rev and cutting depth of 0.45 mm. The predicted responses are Ra = 0.45µm with desirability value of 1.00 which is chosen according to Eq. (7) as shown in Fig. 24 which presents a solution ramps of multi-objective optimization for case (3).

**Table 7**  
Goals and parameter ranges for optimization of cutting conditions

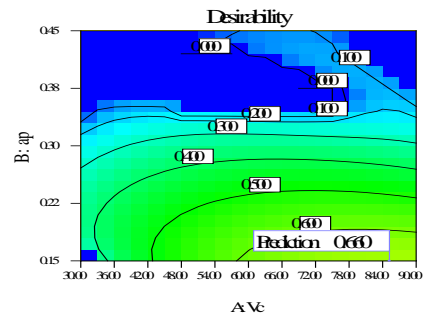
(a) Case 1						
Name	Goal	Lower Limit	Upper Limit	Lower Weight	Upper Weight	Importance
Vc	in range	30	90	1	1	3
ap	in range	0,15	0,45	1	1	3
f	in range	0,08	0,16	1	1	3
Ra	minimize	0,46	1,86	1	1	3
Fa	minimize	22,25	101,22	1	1	3
Fr	minimize	63,56	137,89	1	1	3
Fv	minimize	53,92	234,88	1	1	3
MRR	maximize	0,54	4,86	1	1	3
Pc	minimize	53,92	276,73	1	1	3
(b) Case 2						
Vc	in range	30	90	1	1	3
ap	in range	0,15	0,45	1	1	3
f	in range	0,08	0,16	1	1	3
Ra	minimize	0,46	1,86	1	1	5
Fa	none	22,25	101,22	1	1	
Fr	none	63,56	137,89	1	1	
Fv	none	53,92	234,88	1	1	
MRR	maximize	0,54	4,86	1	1	3
Pc	none	53,92	276,73	1	1	
(c) Case 3						
Vc	in range	30	90	1	1	3
ap	in range	0,15	0,45	1	1	3
f	in range	0,08	0,16	1	1	3
Ra	minimize	0,46	1,86	1	1	5
Fa	none	22,25	101,22	1	1	
Fr	none	63,56	137,89	1	1	
Fv	none	53,92	234,88	1	1	
MRR	none	0,54	4,86	1	1	
Pc	none	53,92	276,73	1	1	

Design-Expert® Software  
Factor Coding: Actual  
Desirability  
1.000  
0.000  
X1 = A: Vc  
X2 = B: ap  
Actual Factor  
C: f = 0.16



(a)

Design-Expert® Software  
Factor Coding: Actual  
Desirability  
1.000  
0.000  
X1 = A: Vc  
X2 = B: ap  
Actual Factor  
C: f = 0.16



(b)

**Fig. 19.** 3D surface plot (a) and contour plot (b) for Desirability case (1)

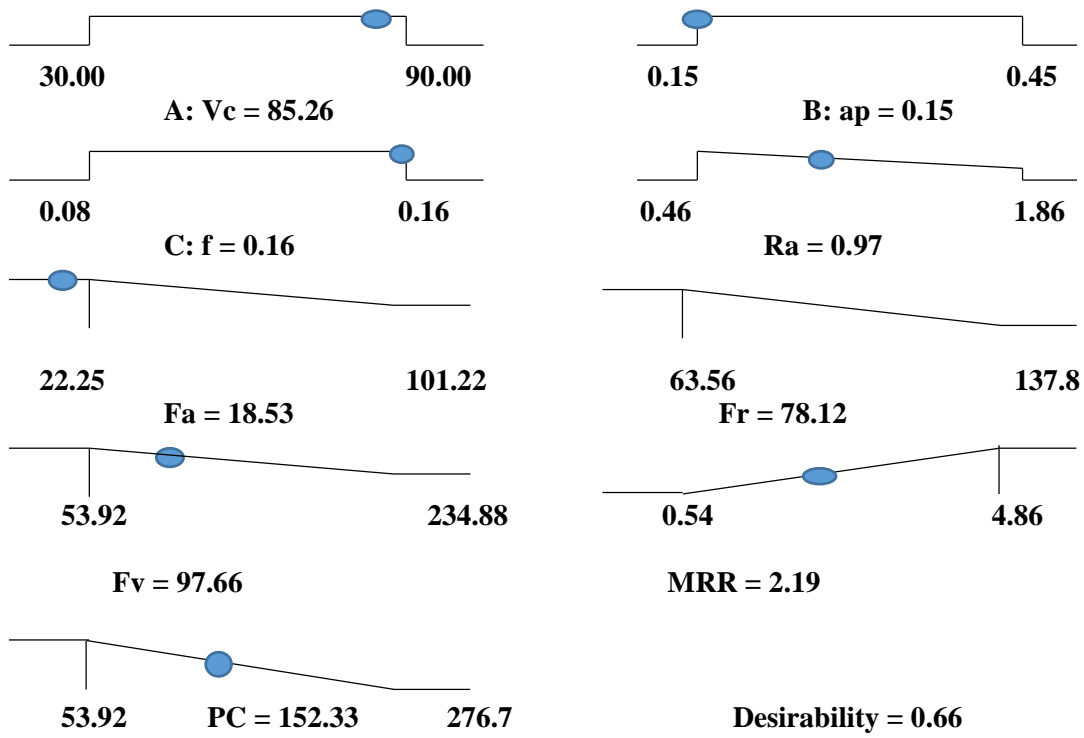


Fig. 20. Solution Ramps of multi-objective optimization for case (1)

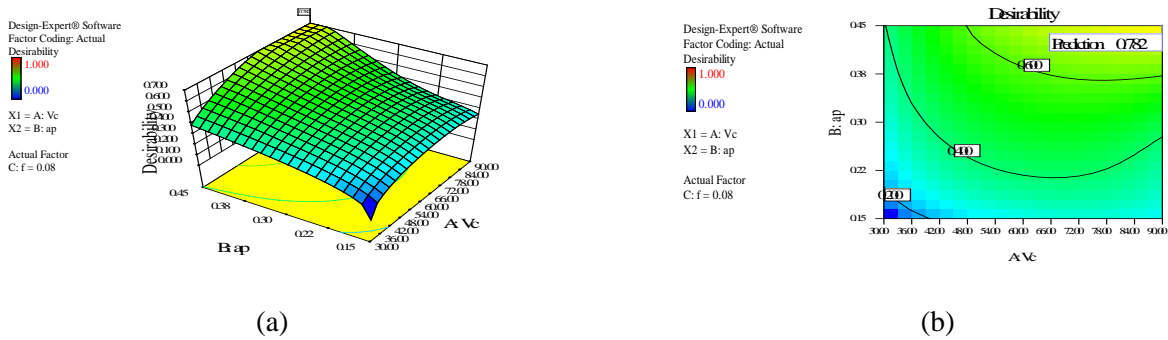


Fig. 21. 3D surface plot (a) and contour plot (b) for Desirability case (2)

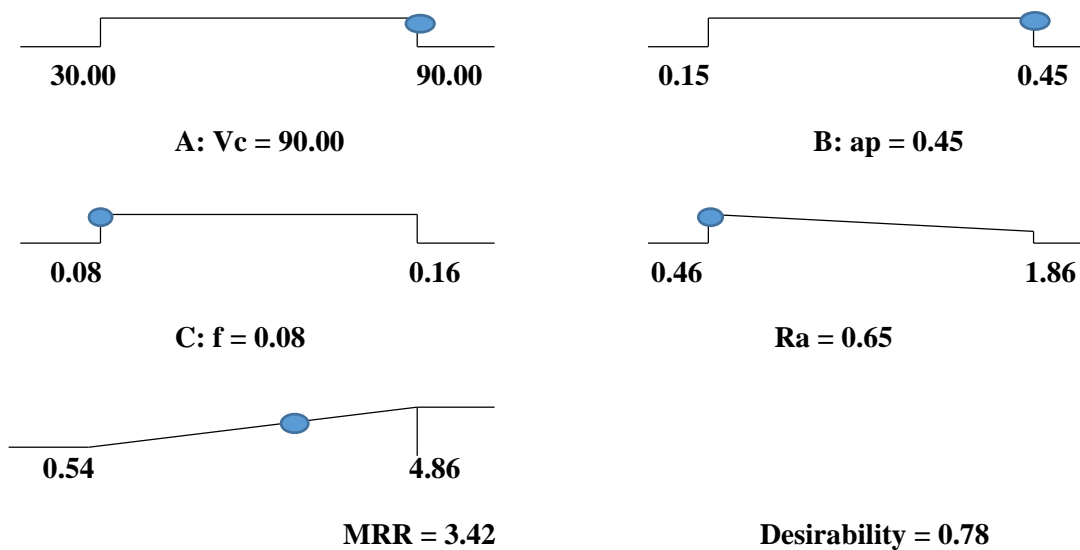
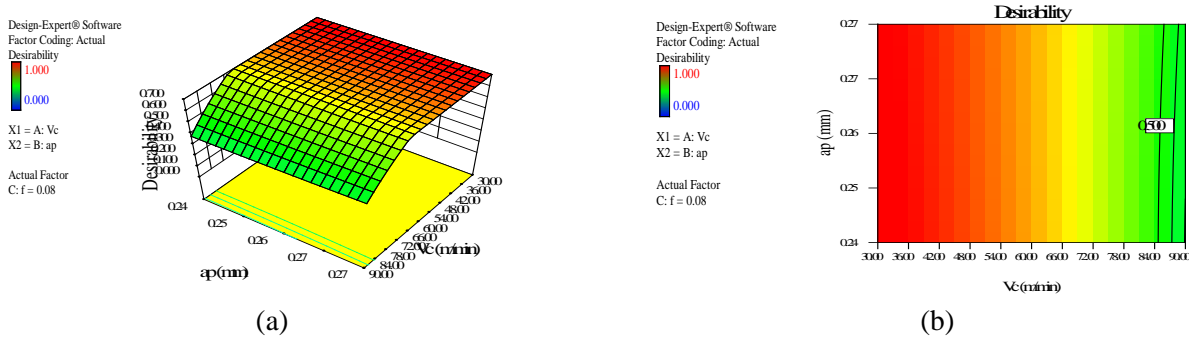
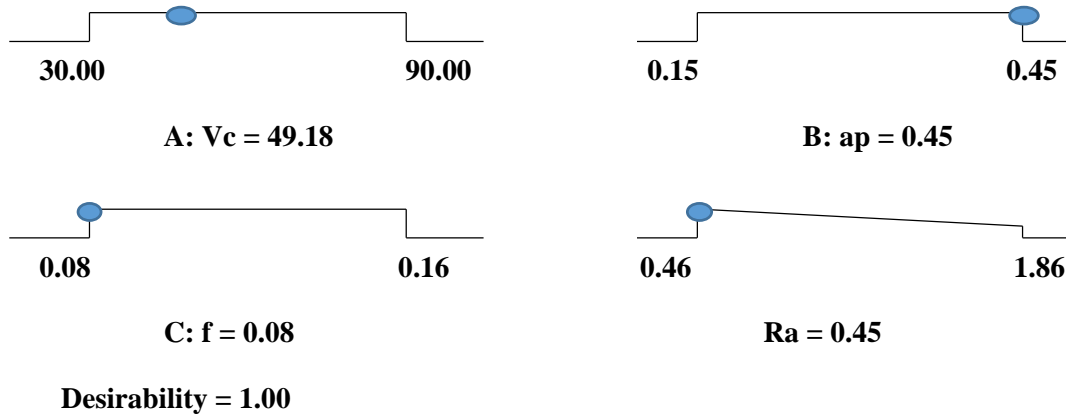


Fig. 22. Solution Ramps of multi-objective optimization for case (2)



**Fig. 23.** 3D surface plot (a) and contour plot (b) for Desirability case (3)



**Fig. 24.** Solution Ramps of multi-objective optimization for case (3)

## 5. Conclusions

The current investigation was based on RSM using Box-Cox plots for developing mathematical models and proving their normality. The desirability approach was followed to optimized surface roughness, cutting forces, productivity and power consumption based on cutting parameters (cutting speed, feed rate and depth of cut). The important findings can be summarized as follows:

1. Feed rate and cutting speed have the greatest influences on surface roughness which accounts 43.58 and 23.85 %, respectively.
2. Cutting force components increase almost linearly as the depth of cut or feed rate increases.
3. Depth of cut has the greatest significance on force components with the contribution values of 79.87, 66.92 and 66.29% on  $F_a$ ,  $F_r$  and  $F_v$ , respectively, followed by feed rate which accounts 1.34, 19.69 and 23.54% on  $F_a$ ,  $F_r$  and  $F_v$ , respectively.
4. The tangential force component presents higher values followed by the thrust and feed force.
5. Cutting speed and depth of cut have the highest significance on productivity with contribution values of 37.31 % for each one.
6. Cutting speed and depth of cut have the highest significance on productivity with contribution values of 38.35 and 34.32 %, respectively.
7. Based on mathematical models obtained using Box-Cox plot for developing and normality proving, it can be concluded that an improvement in surface quality has been observed at the lowest cutting speed, feed rate and depth of cut. Cutting forces are lower for low cutting speed,

high depth of cut and feed rate. In addition, high productivity implies the highest cutting speed, feed rate and depth of cut. Consequently, in the similar conditions, the power consumption will be higher.

8. Based on mathematical models obtained using Box-Cox plot for developing and normality proving, comparisons of experimental and predicted values of the surface roughness, cutting forces, productivity and power consumption show that a good agreement has been achieved between them.
9. Multi-objective optimization cases show that the better surface finish is accompanied by low productivity and the opposite holds. Indeed, for case 1, the roughness obtained is to 0.97  $\mu\text{m}$  with productivity of 2.19  $\text{cm}^3/\text{min}$  using a power of 152.33 when dry turning of Inconel 718 with optimal combination of cutting parameters of 85.26 m/min for  $V_c$ , 0.15 mm for  $ap$  and 0.16 mm/rev for  $f$ . Concerning case 2, an improvement has been found in surface finish by 32.98 % and decreasing in productivity by 35.96 % compared with case 1 when dry turning of Inconel 718 with optimal combination of cutting parameters of 90.00 m/min for  $V_c$ , 0.45 mm for  $ap$  and 0.08 mm/rev for  $f$ . For the case 3, surface finish improved by 53.60 % compared with case 1 when dry turning of Inconel 718 with optimal combination of cutting parameters of 49.18 m/min for  $V_c$ , 0.45 mm for  $ap$  and 0.08 mm/rev for  $f$ .

Regarding the current investigation, the multi-objective optimization methodology proposed can be considered as a powerful approach based on an improved modeling step for the best correlation, and can offer to scientific researchers as well industrial metalworking a helpful Multi-objective optimization procedure for various combinations of input (Workpiece hardness, tool material, cooling ...) and output (surface finish, productivity, surface integrity ...) parameters of machining process.

## Acknowledgements

This work was achieved in the laboratories LMS (University of Guelma Algeria) in collaboration with Acoustic Vibration Laboratory (INSA-Lyon, France). The authors would like to thank the Algerian Ministry of Higher Education and Scientific Research (MESRS) and *the Delegated Ministry for Scientific Research (MDRS)* for granting financial support for CNEPRU Research Project, CODE: A11N01UN240120140013 (University 08 May 1945, Guelma).

## References

- Alauddin, M., El Baradie, M. A., & Hashmi, M. S. J. (1996). Optimization of surface finish in end milling Inconel 718. *Journal of Materials Processing Technology*, 56(1), 54-65.
- Arunachalam, R. M., Mannan, M. A., & Spowage, A. C. (2004). Surface integrity when machining age hardened Inconel 718 with coated carbide cutting tools. *International Journal of Machine Tools and Manufacture*, 44(14), 1481-1491.
- Biksa, A., Yamamoto, K., Dosbaeva, G., Veldhuis, S. C., Fox-Rabinovich, G. S., Elfizy, A., ... & Shuster, L. S. (2010). Wear behavior of adaptive nano-multilayered AlTiN/MexN PVD coatings during machining of aerospace alloys. *Tribology International*, 43(8), 1491-1499.
- Bushlya, V., Zhou, J. M., Lenrick, F., Avdovic, P., & Ståhl, J. E. (2011). Characterization of white layer generated when turning aged Inconel 718. *Procedia Engineering*, 19, 60-66.
- Chen, Y. C., & Liao, Y. S. (2003). Study on wear mechanisms in drilling of Inconel 718 superalloy. *Journal of Materials Processing Technology*, 140(1), 269-273.
- Choudhury, I. A., & El-Baradie, M. A. (1999). Machinability assessment of inconel 718 by factorial design of experiment coupled with response surface methodology. *Journal of Materials Processing Technology*, 95(1), 30-39.

- Davim, J. P., Gaitonde, V. N., & Karnik, S. R. (2008). Investigations into the effect of cutting conditions on surface roughness in turning of free machining steel by ANN models. *Journal of Materials Processing Technology*, 205(1), 16-23.
- Devillez, A., Le Coz, G., Dominiak, S., & Dudzinski, D. (2011). Dry machining of Inconel 718, workpiece surface integrity. *Journal of Materials Processing Technology*, 211(10), 1590-1598.
- Dudzinski, D., Devillez, A., Moufki, A., Larrouquere, D., Zerrouki, V., & Vigneau, J. (2004). A review of developments towards dry and high speed machining of Inconel 718 alloy. *International Journal of Machine Tools and Manufacture*, 44(4), 439-456.
- Ezugwu, E. O., & Bonney, J. (2004). Effect of high-pressure coolant supply when machining nickel-base, Inconel 718, alloy with coated carbide tools. *Journal of Materials Processing Technology*, 153, 1045-1050.
- Gaitonde, V. N., Karnik, S. R., Figueira, L., & Davim, J. P. (2009). Machinability investigations in hard turning of AISI D2 cold work tool steel with conventional and wiper ceramic inserts. *International Journal of Refractory Metals and Hard Materials*, 27(4), 754-763.
- Guo, Y., Loenders, J., Duflou, J., & Lauwers, B. (2012). Optimization of energy consumption and surface quality in finish turning. *Procedia CIRP*, 1, 512-517.
- Hessainia, Z., Belbah, A., Yallese, M. A., Mabrouki, T., & Rigal, J. F. (2013 b). On the prediction of surface roughness in the hard turning based on cutting parameters and tool vibrations. *Measurement*, 46(5), 1671-1681.
- Jawaid, A., Koksai, S., & Sharif, S. (2001). Cutting performance and wear characteristics of PVD coated and uncoated carbide tools in face milling Inconel 718 aerospace alloy. *Journal of Materials Processing Technology*, 116(1), 2-9.
- Krain, H. R., Sharman, A. R. C., & Ridgway, K. (2007). Optimisation of tool life and productivity when end milling Inconel 718TM. *Journal of Materials Processing Technology*, 189(1), 153-161.
- Li, H. Z., Zeng, H., & Chen, X. Q. (2006). An experimental study of tool wear and cutting force variation in the end milling of Inconel 718 with coated carbide inserts. *Journal of Materials Processing Technology*, 180(1), 296-304.
- Lynch, C. T. (1989). *Practical handbook of materials science*. CRC press.
- Maiyar, L. M., Ramanujam, R., Venkatesan, K., & Jerald, J. (2013). Optimization of machining parameters for end milling of Inconel 718 super alloy using Taguchi based grey relational analysis. *Procedia Engineering*, 64, 1276-1282.
- Myers, R. H., Montgomery, D. C., & Anderson-Cook, C. M. (2009). *Response surface methodology: process and product optimization using designed experiments* (Vol. 705). John Wiley & Sons.
- Nalbant, M., Altın, A., & Gökkaya, H. (2007). The effect of coating material and geometry of cutting tool and cutting speed on machinability properties of Inconel 718 super alloys. *Materials & Design*, 28(5), 1719-1724.
- Ng, E. G., Lee, D. W., Dewes, R. C., & Aspinwall, D. K. (2000). Experimental evaluation of cutter orientation when ball nose end milling Inconel 718<sup>TM</sup>. *Journal of Manufacturing Processes*, 2(2), 108-115.
- Osborne, J. W. (2010). Improving your data transformations: Applying the Box-Cox transformation. Practical Assessment, *Research & Evaluation*, 15(12), 1-9.
- Outeiro, J. C., Pina, J. C., M'saoubi, R., Pusavec, F., & Jawahir, I. S. (2008). Analysis of residual stresses induced by dry turning of difficult-to-machine materials. *CIRP Annals-Manufacturing Technology*, 57(1), 77-80.
- Pawade, R. S., Joshi, S. S., Brahmankar, P. K., & Rahman, M. (2007). An investigation of cutting forces and surface damage in high-speed turning of Inconel 718. *Journal of Materials Processing Technology*, 192, 139-146.
- Rahman, M., Seah, W. K. H., & Teo, T. T. (1997). The machinability of Inconel 718. *Journal of Materials Processing Technology*, 63(1), 199-204.
- Ramanujam, R., Venkatesan, K., Saxena, V., & Joseph, P. (2014). Modeling and optimization of cutting parameters in dry turning of Inconel 718 using coated Carbide Inserts. *Procedia Materials Science*, 5, 2550-2559.

- Sadat, A. B. (1987). Surface region damage of machined inconel-718 nickel-base superalloy using natural and controlled contact length tools. *Wear*, 119(2), 225-235.
- Sahoo, A., & Mishra, P. (2014). A response surface methodology and desirability approach for predictive modeling and optimization of cutting temperature in machining hardened steel. *International Journal of Industrial Engineering Computations*, 5(3), 407-416.
- Sakia, R. M. (1992). The Box-Cox transformation technique: a review. *The Statistician*, 41(2), 169-178.
- Sandvik., C. (2009). *Catalogue General, Outils de coupe Sandvik Coromant, Tournage – Fraisage – perçage – Alésage – Attachements*.
- Sharman, A. R. C., Hughes, J. I., & Ridgway, K. (2015). The effect of tool nose radius on surface integrity and residual stresses when turning Inconel 718™. *Journal of Materials Processing Technology*, 216, 123-132.
- Settineri, L., Faga, M. G., & Lerga, B. (2008). Properties and performances of innovative coated tools for turning inconel. *International Journal of Machine Tools and Manufacture*, 48(7), 815-823.
- Ståhl, J. E., Schultheiss, F., & Hägglund, S. (2011). Analytical and experimental determination of the Ra surface roughness during turning. *Procedia Engineering*, 19, 349-356.
- Thakur, D. G., Ramamoorthy, B., & Vijayaraghavan, L. (2009). Study on the machinability characteristics of superalloy Inconel 718 during high speed turning. *Materials & Design*, 30(5), 1718-1725.
- Zahia, H., Nabil, K., MA, Y., Mabrouki, T., Ouelaa, N., & Rigal, J. F. (2013 a). Turning roughness model based on tool-nose displacements. *Mechanics*, 19(1), 112-119.
- Zahia, H., Athmane, Y., Lakhdar, B., & Tarek, M. (2015). On the application of response surface methodology for predicting and optimizing surface roughness and cutting forces in hard turning by PVD coated insert. *International Journal of Industrial Engineering Computations*, 6(2), 267-284.